Eurasian Chemico-Technological Journal 17 (2015) 267-274

# Structure of Core-Shell Ni/Au Nanoparticles Synthesized in Two-Stage Process From Aqueous Salt Solutions

**Yu.A. Zaharov[1,2*], V.G. Dodonov[1], V.M. Pugachev[1], D.M. Russakov[1], N.V. Ivanova[1], R.P. Kolmykov[1], N.K. Yeremenko[2], I.I. Obraztsova[2]**

[1]Kemerovo State University, Krasnaya st., 6, 650043 Kemerovo, Russia
[21]Institute of Coal Chemistry and Material Science SB RAS, pr. Sovetskiy 18, 650000 Kemerovo, Russia

**Article info**

*Received:*
25 May 2015
*Received and revised form:*
18 July 2015
*Accepted:*
20 August 2015

**Abstract**

Core-shell Ni/Au nanoparticles are synthesized in a two-stage process in aqueous solutions. The core-shell structure of the synthesized particles is proven by using results of HRTEM, TEM, SAXS and CVA methods. The thickness of the core is estimated at 1 nm and it is formed from 1–2 layers of mutually oriented gold crystallites. The CVA results show that the Au-shells are nanoporous, and that a layer of nickel oxidation products is formed. These results were obtained by using Vis spectrophotometer, TEM, HRTEM, SAXS, CVA and elemental analysis.

## 1. Introduction

Nanosized systems of the metals of the iron group/noble metals (Au, Pt, Ag) with a core-shell structure are enjoying increasing applications in medicine, biology, magnitotechnique and microelectronics [1–6]. Development of new simple and effective methods for the synthesis of such systems is of particular importance.

Most synthetic methods (Fe, Co, Ni/Au, Ag) [7–15] are carried out in non-aqueous conditions. They are difficult to realize and there is limited information about the morphological characteristics of these particles. There is a need for a more detailed study of the structural features and composition of the particles: shell continuity and its efficiency in core protection against corrosion; existence of reducing agents and metal cores oxidation products in particles; possible formation of mixed nanophases at the interfaces of the core-shell and complication of the particle structure caused by these processes.

### *Synthesis and methods of materials investigation*

Analytical grade $NiSO_4$, sodium citrate, $NaBH_4$ and $HAuCl_4 \cdot 4H_2O$ were used without additional purification. Bidistilled water was used.

The synthesis involves the combination of a galvanic displacement reaction between $HAuCl_4$ and Ni nanoparticles ($Ni^0 + Au^{+3} \rightarrow Ni^{+2} + Au^0$) and reduction of $HAuCl_4$ by remaining $NaBH_4$ after generation of Ni nanoparticles [12, 16].

In a typical experiment (12 ± 1 °C), 25 ml of water was added to aqueous solutions of $NiSO_4$ (0.5 ml, 0.1 M) and sodium citrate (0.5 ml, 0.1 M). Afterwards, 1 ml of freshly prepared $NaBH_4$ (0.1 M) was added dropwise but rapidly for 20 min into the stirring system. The complete reduction was controlled by verifying the absence of the surface plasmon resonance band for $NiSO_4$ in the visible spectrum range.

Then, 20 min later, aqueous $HAuCl_4$ solution (0.5 ml, 0.1 M) was added in two stages. First 2–3 drops of $HAuCl_4$ were added and 10 min later the remaining quantity of $HAuCl_4$ was added to obtain a stable Au-shell over Ni nanoparticles. The solution was kept stirring for 30 min. A complete reduction was controlled by verifying the absence of the surface plasmon resonance band for $NiSO_4$ in the visible spectrum range.

Vis absorption spectra were recorded with a PE-5400V spectrophotometer. XRD patterns were recorded with a X-ray diffractometer DIFRAY-401 (iron radiation). Quantitative analysis of the elemental composition was acquired by using optical emission spectroscopy (OES) in an inductively coupled plasma spectrometer iCAP-6500 DUO. Three aliquots 0.1 ml Ni/Au were taken. Samples were

* Corresponding author. E-mail: zaharov@kemsu.ru

transferred to the measuring tubes (50 ml), and aqua regia (2 ml) was added. After complete dissolution of the particles the measuring tubes were filled with distilled water up to the maximum mark. The resulting solution was injected into the spectrometer atomization unit and they were analyzed with a sample flow rate of 1.0 ml/min. Spectrometer calibration was carried out by using standard solutions gold ions (0.1 mg/cm$^3$) and nickel ions (1 mg/cm$^3$). The resulted calibration curves were described by a linear equation with a correlation coefficient equal to 1 (standard deviation from the linear dependence is 0.001).

An investigation of the electrochemical response of the Ni/Au particles was carried out by means of cyclic voltammetry with a potentiostat/galvanostat PARSTAT 4000 in a three-electrode cell. Ni/Au particles, preliminary cleaned by water or etching agents, were immobilized on the surface of a carbon paste electrode fabricated from chemical pure graphite powder (C3) and paraffine oil. Counter and reference electrodes were platinum wire and Ag, AgCl/0.1 M KCl respectively. All voltammetric experiments were performed in 0.1 M KCl solution with addition of HCl (pH = 2.5) as background electrolyte. ICP atomic emission spectroscopy was used for the determination of the elements (Ni, Au, B) concentrations in the etching solutions.

Small-angle X-ray scattering (SAXS) measurements were carried out using KRM-1 diffractometer in the iron characteristic radiation by counting the pulses in discrete points in the range of 0.002–0.348 Å$^{-1}$. The particle size distribution functions were computed from the SAXS curves in the approximation of homogeneous spheres and the «core-shell» model. The computer treatment of experimental data (collimation correction, calculation of particle size distribution functions) was carried out according to computer programs created by the authors [17]. For the SAXS measurements the investigated powders were glued as a thin layer (~ 50–100 microns) on lavsan film so that their surface density, estimated from X-ray absorption was 0.7–0.8 or 3–4 mg/cm$^2$.

TEM images were acquired by using a transmission electron microscope JEM – 2100.

## 2. Experimental

### *2.1. Electron microscopy*

Typical TEM micrographs of Ni/Au nanoparticles obtained in this work are shown in Fig. 1a–b. High resolution TEM micrographs are shown in Fig. 1c.

It can be seen that the particles have a tendency to form filamentous and coalescence forms (aggregation). Non-aggregated particles have a spherical shape, a slight variation in size (see the size distribution histogram in Fig. 1b) and a «core-shell» structure.

The brighter shade of the Au-shell is associated with a greater scattering of the electrons in gold, and the observed image contrast suggests that the Ni-cores are sphere-like, with a (diameter between 4 and 8 nm), a thickness of the Au-shell of about 1 nm and the average for an array of 100 particles gives a nickel content of 20–35 wt.% (in the approximation of an absence of nickel oxidation products).

The images of the particles show the atomic planes with distinct atomic rows. In some cases they form a regular hexagonal structure with the (111) planes of densest packing. The measured interatomic spacing of 0.288 nm is in good agreement with the calculated lattice parameters of 0.2884 nm for gold. There is also a good agreement between the measured spacing rows 0.250 nm and the value of 0.2498 nm inherent to the gold lattice. At an inclinated view of the 111 planes the hexagonal pattern disappears because the particles are spherical and the rows can only be visually distinguished in one direction. The spacing between them is reduced in such a projection, depending on the angle of inclination to 0.22–0.24 nm or less.

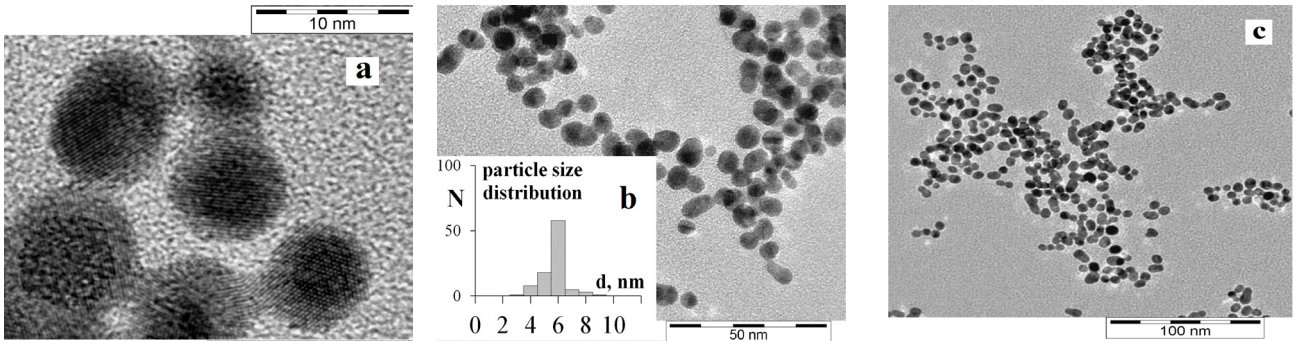


Fig. 1. TEM (a, b) and HRTEM (c) images of Ni/Au nanoparticles. Insert in 1b: size distribution histogram.

Occasionally there are particles with a spacing between the rows of 0.26–0.28 nm and 0.16–0.20 nm. Both groups are well matched to the distances between the atomic rows of gold at oblique arrangement of the (200) planes already mentioned above (0.2884 nm interatomic spacing) and $d_{200}$ (0.2039 nm). Thus, the surface of the Au-shell is presented as the main plane of the type (111) (octahedron) and (200) (cc), which are the most typical ones in the formation of crystals with the FCC lattice. At the same time there are particles which have not ordered nanocrystals in the Au-shells. Although of nanometer thickness, the Au-shell is substantially continuous and covers the whole or a part of the bulk surface Ni-core in according to the HTEM micrographs. Occasionally there is no fixed gold on the observed area because of the FCC lattice interplanar spacings specified above. An absence of surfactants leads to some aggregation of the particles (Fig. 2).

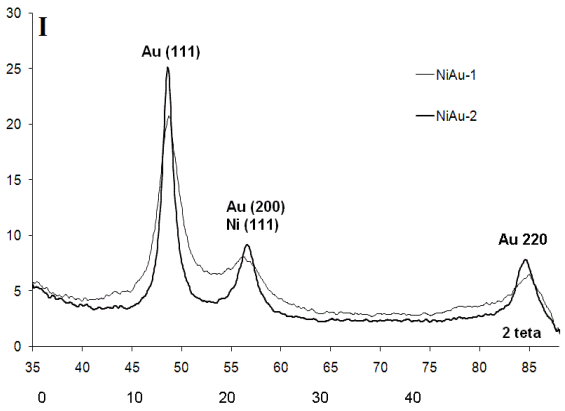


Fig. 2. X-ray powder pattern of Ni/Au system. 1 – Ni-core sizes 4–8 nm, 2 – Ni-core sizes near 12 nm.

### *2.2. X-ray analysis*

Only the basic reflections of gold are seen in the X-ray patterns of the Ni/Au powders (Fig. 2).

In according with the considerably lower diffusing capacity of nickel compared to gold, the relatively low content in the particles (1.1, 1.4, 1.6) and a strong broadening of the reflections (due to the nanodimension of the core and the shell) it is not possible to find even the strongest nickel reflection (111) on a background of the (200) gold reflection. As such it is also impossible to distinguish the weaker nickel reflection of (200) at 66.9°, not even in samples Ni/Au with a Ni-core size 2–3 times larger than that of the standard sample (12 nm see Fig. 2). The phases of possible oxidation products of nickel are not detected.

An average crystallite size is measured by Scherrer broadening of the (111) gold reflection for the standard and the samples having a large size Ni-core. The results are 2 and 10–12 nm, respectively. However, the average size consists of the three contributing relatively large size in the direction roughly along the shell and a smaller one, which is its thickness. As a result, the true thickness may be only half of the average, or even less.

### *2.3. Elemental composition of particles*

The analysis is realized for three identical samples; for each basic element it was carried out with three wavelengths (197.82; 201.20 and 242.79 nm for Au; 221.68; 232.0 and 361.94 nm for Ni).

The results are shown in Table 1.

**Table 1**

The results of elemental composition of particles

| Sample | W (Ni), % | W (Au), % |
|---|---|---|
| 1 | 42.5 | 57.5 |
| 2 | 42.8 | 57.2 |
| 3 | 42.6 | 57.3 |
| Average | 42.7 ± 0.5 | 57.3 ± 0.5 |

W – mass % of Ni and Au

### *2.4. Cyclic voltammetry*

Electrochemical measurements were performed in the following steps:

1. Cyclic voltammograms (CV) scanning in the nickel oxidation area (–0.6 ÷ 0.2 V) with increasing of the maximum potential up to +0.8 V (step of 0.2 V).
2. Cathodic reduction at –1.5 V CV and CV scanning in the potential window –0.6 ÷ 0.2 V.
3. CV scanning in the potential window –0.6 ÷ 0.95 V, in this case the gold oxidation area is reached.
4. Preliminary anodic oxidation of gold at +1 ÷ +1.3 V during 10 s and CV scanning (–0.6 ÷ 1.2 V) including the stage of cathodic reduction at –1.5 V.

The typical (CV) are represented in Fig. 3. The absence of the nickel oxidation peak near –0.3 V (step 1 of the electrochemical measurements) indicates the absence of nickel available for the electrolyte, including the Ni located at the surface of the Au-shell. That generally corresponds to the conditions (reaction sequences) of synthesis of Ni/Au particles.

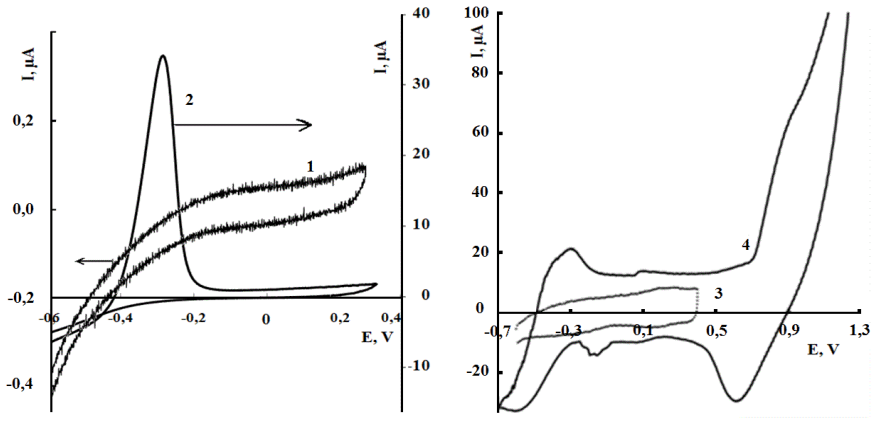


Fig. 3. Cyclic voltammogramms for the Ni/Au samples. Numbers (1, 2, 4) corresponds to the steps of the electrochemical measurements (see explanation in text). Curve 3 – CV obtained after sample etching in ammoniacal solution.

The presence of a reproducible nickel oxidation peak in the second step of measurements (after cathodic reduction) clearly indicates the presence of oxidized forms of Nickel (NiO, $Ni(OH)_2$) in the Ni/Au particles. These compounds may be located on the outer surface of Au-shell or, in view of its discontinuity, in the nanopores of the shell or on the outer surface of the Ni-core and prevent access of the electrolyte to the Ni-core, thus blocking the processes of anodic oxidation of nickel during the first step of the experiment. Within the cathodic half-cycle the oxidized forms are reduced to nickel or dissolve in the acidic electrolyte to enhance the cathodic nickel crystallization, which is oxidized in the anodic half-cycle, as is demonstrated by the corresponding peak (Fig. 3).

CV obtained at the maximum potential window after reduction at –1.5 V (fourth step of measurements) shows no increase of the nickel oxidation peak.

After an etching pretreatment of the initial Ni/Au samples in a 4 M $NH_3$ (or 2.5 M HCl) solution this anodic peak on CV is not observed. This suggests the chemical dissolution of the Ni-core and its oxidized forms at the previous stages of experiments to be almost complete.

The analysis of the etching solutions (containing $NH_3$ or HCl) by atomic emission spectroscopy confirms the discontinuity of the Au-shell and, therefore, the dissolution of the Ni-core and the presence oxide-hydroxide nanoinclusions.

It is shown that the preliminary etching treatment in $NH_3$ or HCl solutions during 15 and 6 min respectively leads to a complete removal of nickel from the analyzed samples (Fig. 4). In this case peaks of anodic oxidation and cathodic deposition of nickel are not observed on the CV. These results suggest that the electrochemical detection of oxide-hydroxide nanophases in CV experiments occurs predominantly by dissolution in acidic electrolyte.

In the potential range of 0.6÷0.8 V the processes, probably, corresponding to oxidation-reduction of bimetallic phases $Au_xNi_y$ (rich in gold) were observed; the formation of these phases does not contradict the Au-Ni phase diagram [19].

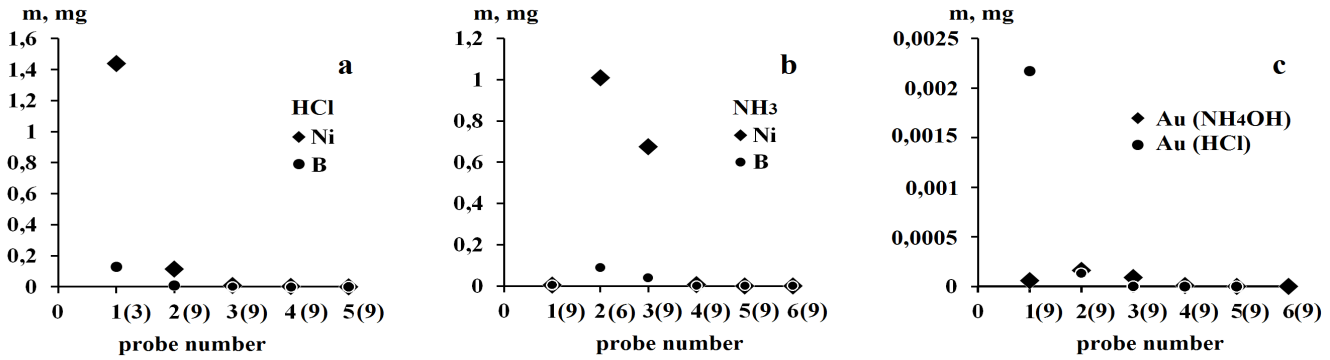


Fig. 4. Nickel and boron contents in the etching solutions: 2.5 M HCl (a); 4.5 M $NH_4OH$ (b); gold content (c) as a function of quantity of consecutive etching operations (duration in minutes indicated in brackets).

This assumption was confirmed by the OES-analysis of the etching solutions (Fig. 4c). It is known, that dissolution of low-dimensional gold particles in the HCl does not occur. At the same time, during etching of the Ni/Au particles, gold was detected in amounts ≈ 0.2÷0.4 wt.% of dissolved nickel, and besides, mostly after the first etching. This fact means that Au-containing nanophase ($Au_xNi_y$) is located on the Ni-core surface, i.e. on the boundary with Au-shell.

It should be noted that in the samples significant amounts of boron and (or) its compounds were detected (Fig. 4). The presence of boron impurities ($BO_3^-$, $BO_2^-$) in the transition metals nanoparticles prepared by reduction of aqueous solutions of alkali metal tetrahydroborates was described in a number of papers (see, for example [20]), but it was not observed in [7] during the synthesis of Ni/Au core-shell.

### *2.5. Small-angle X-ray scattering*

Experimental SAXS curves for Ni/Au samples with different surface densities are shown in Fig. 5. After the transformation to a common scale these SAXS curves are nearly identical, an indication for the absence of multiple scattering effects.

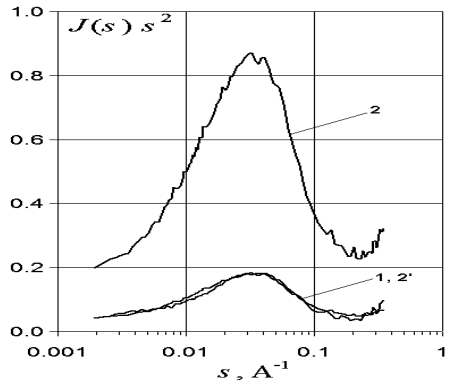


Fig. 5. Raw SAXS experimental curves (slit collimation) for Au/Ni samples with a surface density of 0.5 mg/cm$^2$ (1) and 2.3 mg/cm$^2$ (2); 2' - $J(s)$ curve 2×0.22.

Size distribution functions of inhomogeneities (SDFI) computed from the SAXS curves for different variants of particles structure are shown in Fig. 6. A comparison of experimental SAXS curves with theoretical ones for different model types is shown in Fig. 7.

The calculations performed in the approximation of homogeneous spherical particles, i.e. in the presentation of the investigated system as a nano-heterogeneous particle mixture of gold and nickel, allows to describe the experimental SAXS data only by the bimodal SDFI. This does not correspond to the results of HTEM and cyclic voltammetry (1, 4): the analysis of photomicrographs shows the absence of particles with sizes corresponding to the position of an additional maximum on SDFI (about 2.5 nm), and the CVA curves in the anode region have no peaks of metallic nickel oxidation.

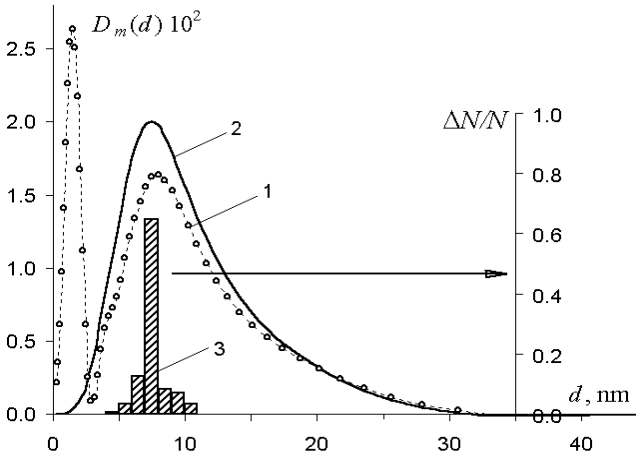


Fig. 6. Size distribution functions $D_m(d)$ of inhomogeneities (SDFI) for the system Ni/Au: 1 – computed by homogeneous spheres; 2 – computed by three-phase shell-core model Ni|$Ni(OH)_2$/Au; 3 – histogram of particle size distribution obtained from TEM results.

The results of computer simulation have shown that additional maximum on SDFI obtained in the approximation of homogeneous spherical particles, can also be explained by the presence of an external particle shell with a density greater than the density (e.g. gold) of their inner core [18].

Electrochemical experiments (see Par. 4), however, indicate also the presence of products of nickel oxidation in the particles. This fact is consistent with the SAXS results: the observed intensity of the additional peak on SDFI connected with the presence of a shell with a higher scattering density is lower than it should be for a rigorously two-phase Ni-Au core-shell structure. This may be due to the presence of a third phase in the form of a less dense shell (NiO, $Ni(OH)_2$) which partially offsets the contribution of a gold shell in the SAXS amplitude.

Computer simulation has shown that the results of SDFI calculations in terms of a nano-heterogeneous three layer particle model are in agreement with the experiment, as the monomodal particle size distribution shows a good agreement between the experimental and calculated SAXS curves (Fig. 7 – solid line). Simulation was carried out using the

known values of electron densities ($\rho_e$, $e/Å^3$) of the phases in crystalline state making up the particles ($\rho_{Au} = 4.71$, $\rho_{Ni} = 2.56$, $\rho_{NiO} = 1.98$, $\rho_{Ni(OH)_2} = 1.18$) as a Ni-core and surrounding spherical Au-shell (that corresponds to HTEM results) and an additional $Ni(OH)_2$ or $Ni(OH)_2$ + NiO shell, presumably in a form of a spherical layer. Two variants of the spatial organization of particles were considered: Ni/$Ni(OH)_2$ or NiO + $Ni(OH)_2$/Au and Ni/Au/$Ni(OH)_2$ or NiO + $Ni(OH)_2$. The dimensional particle characteristics corresponding to the positions of maximum of SDFI (Fig. 6) and the average Ni-core sizes for which the function is monomodal and the best agreement between the experimental and theoretical SAXS curves is observed (Fig. 7) are shown in Table 2 (in nm).

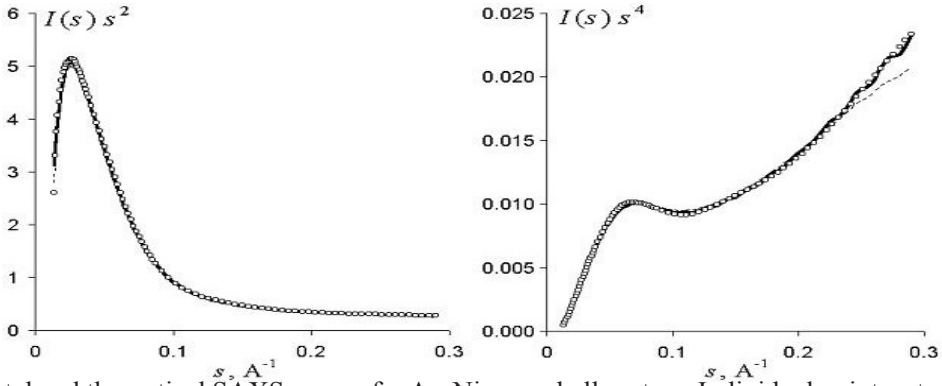


Fig. 7. Experimental and theoretical SAXS curves for Au-Ni core-shell system. Individual points – treated experimental values (with smoothing and collimation correction); dotted line – homogeneous spheres approximation corresponding to a bimodal $D_m(d)$. function; solid line – three-phase core-shell model approximation Ni/$Ni(OH)_2$/Au, corresponding to a mono-modal $D_m(d)$ function.

**Table 2**
Dimensional particle characteristics estimated from SAXS

| Model parameters | Diameter of particles | | Diameter of Ni-core | | Thickness of oxide/ hydroxide shell | | Thickness of Au-shell | |
|---|---|---|---|---|---|---|---|---|
| Estimation method | By average value for the SDFI first mode | By the position of SDFI maximum | By average value for the SDFI first mode | By the position of SDFI maximum | By average value for the SDFI first mode | By the position of SDFI maximum | By average value for the SDFI first mode | By the position of SDFI maximum |
| Ni/Au/$Ni(OH)_2$+NiO | 11.0 | 8.9 | 6.6 | 5.4 | 1.1 | 0.89 | 1.1 | 0.81 |
| Ni/$Ni(OH)_2$/Au | 10.5 | 7.5 | 8.3 | 5.9 | 0.50 | 0.40 | 0.60 | 0.40 |
| Ni/$Ni(OH)_2$+NiO/Au | 10.4 | 7.5 | 7.9 | 5.7 | 0.62 | 0.47 | 0.63 | 0.43 |

With the mode of synthesis that was used the formation of a hydroxide or oxide-hydroxide layer as an external particle shell seems unlikely. It might be the result of an electrolytic substitution process ($Ni^0 + Au^{+3} \rightarrow Ni^{+2} + Au^0$), diffusion of Ni + 2 through available nanopores (see Par. 4) of the emerging Au film to the external particle surface followed by their recovery to $Ni^0$ and subsequent nickel oxidation. In this case we have to presume a greater role of the electrolytic replacement even under the condition of parallel reaction of $Au^{+3}$ reduction by sodium tetrahydroborate. The simulation results confirm a small probability of this process: the calculated thickness of the external oxidized shell turns out too large (nearly comparable to the thickness of Au shell in case of Ni $(OH)_2$ + NiO or exceeding it by nearly 2 times for $Ni(OH)_2$), but this is not detected microscopically. Besides the content of nickel in these particles should be less than 25 wt.% which does also not correspond to the analysis of their composition (see Par. 3).

The more likely structure model of the particles is that the Ni core is covered with a layer of $Ni(OH)_2$ or $Ni(OH)_2$ + NiO of unknown continuity and then – an external Au shell. In this case mass fractions of Ni, $Ni(OH)_2$ and Au phases are 40%, 6% and 54% for Ni/$Ni(OH)_2$/Au particles and 34%, 12% and 54% for Ni/$Ni(OH)_2$ + NiO/Au particles respectively (at nickel oxide to nickel hydroxide mass ratio of 1:1) (Fig. 8). The SDFI corresponding to these two versions of particles are nearly identical, and the theoretical curves are nearly equally corresponding to the experimental SAXS curve (Fig. 7).

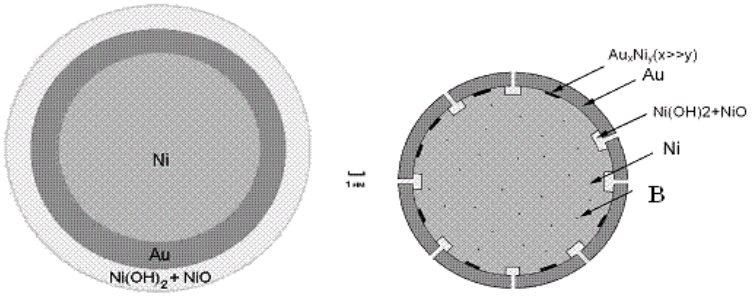


(a) (b)

Fig. 8. The less (a) and the most probable (b) model nanoparticles Ni/Au core-shell, Ni and Au. Schemes are given in the scale according to the results of TEM, SAXS, elemental composition analysis.

The results of the estimation of the particle's dimensional characteristics in function of the assumed models are in agreement with ones obtained by other methods: the SDFI corresponds to the particle size distribution, obtained from HTEM data (Fig. 6), and the total amount of nickel in the particles calculated according to its content in the metallic core and in the $Ni(OH)_2$ or $NiO + Ni(OH)_2$ (1:1) shells with thickness presented in Table 1 is 43 wt.% and 40 wt.% respectively, that is in good agreement with the results of elemental analysis (42.7 wt.% Ni) given in (Par. 3).

The possibility of a complete dissolution of nickel (both in metal and in oxidized state) in ammoniac and acidic media (Par. 4) that was demonstrated, indicates a discontinuity of the Au shell and consequently – the possibility of a partial oxidation of the Ni core during the synthesis or storage of the samples.

## 3. Conclusions

Figure 8 shows the most likely model of the synthesized Ni/Au core-shell particles, in accordance with the experimental results. According to the HR-TEM results the particles are spherical, HRTEM and SAXS results show they have a narrow size distribution (4–8 nm) and TEM, CVA and SAXS demonstrate they have a Ni/Au core-shell structure. Based on the HRTEM results, Au shell consists from nanocrystallites oriented along (111). Taking into account this information and the TEM, and SAXS model results, we can conclude that the average thickness of the Au-shell is about 1 nm.

Comparison of the results from X-ray diffraction (crystallite size measured by Scherrer broadening) with the TEM and SAXS results, suggest that the shell is formed from 1–2 layers of commonly oriented Au crystallites.

CVA results suggests the Au-shells to be nanoporous. As a result, during the synthesis or storing of the samples there is a possible formation of a layer of nickel oxidation products ($Ni(OH)_2$ and $Ni(OH)_2 + NiO$) with an unknown continuity and an average (relative) thickness comparable to the Au-shell. SAXS results indicate this layer is formed on the surface of the Ni-cores and under the Au-shells. According to the CVA results and the analysis of the particles etching solutions it is possible to form $Au_xNi_y$ (x>>y) nanophases in contact with the Ni-Au. Also, elemental analysis of the Ni/Au particles showed the existence of boron impurities (or its compounds) as oxidation products of the $NaBH_4$ that was used in the synthesis.

Thus, these results show that Ni/Au core-shell particles with 1 nm Au-coating have a substantially more complex composition and structure, than suggested in [7, 12, 20 etc.]. These peculiarities may exist in other systems such as the «core (transition metals)/shell noble metals» and it should be considered in their synthesis and in the investigation of their properties.

## Acknowledgments

The present work was supported by the Ministry of Education and Science of the Russian Federation (project 2014/64) and used equipment of the Centre for shared use of scientific equipment of Kemerovo Science Centre of Siberian Branch of the Russian Academy of Sciences. The authors wish to thank A.N. Yeremenko for her help in the translation of this article in English.

## References

[1]. Nanoscience and nanotechnology. Encyclopedia of Life Support Systems. Ed. Osama O. Avadelkarim, Chunli Bay, S.P. Kapitsca, E.E. Demidova. –

Moscow: UNESCO: EOLSS: ID MAGISTR PRESS, 2011. – 1000 p.
[2]. A.A. Eliseev, A.V. Lukashin Functional nano-materials. Ed. Ju.D. Tretjakov. M.: Physmatlit, 2010. - 456 p.
[3]. F.J. Brieler, P. Grundmann, M. Fröba, L. Chen, P.J. Klar, W. Heimbrodt, H.-A. Krug von Nidda, T. Kurz, A. Loidl, Chem. Mater. 17 (4) (2005) 795–803.
[4]. D.K. Yi, S.S. Lee, J.Y. Ying, Chem. Mater. 18 (2006) 2459–2461.
[5]. Gao J, Gu and B. Xu, Acc. Chem. Res. 42 (2009) 1097–1107.
[6]. Jun Y-w, Lee J.H, Cheon J., Angew. Chem. Jnt. Ed, 47 (2008) 5122–5135.
[7]. D. Chen, J. Li, Chunsheng Shi, X. Du, N. Zhao, J. Sheng and S. Liu, Chem. Mater. 19 (2007) 3399–3405.
[8]. S.J. Cho, A.M. Shahin, G.J. Long, Chem. Mater. 18 (2006) 960–967.
[9]. S.J. Cho, J.S. Idrobo, J. Olamit, Chem. Mater. 17 (2005) 3181–3186.
[10]. J. Lin, W.L. Zhou, A. Kumbhar, Solid. State Chem. 159 (2001) 26–31.
[11]. W.-r. Lee, M.G.Kim, J.-r. Choi, J.-I. Park, S.J. Ko, S.J. Oh and J. Cheon, J. Am. Chem. Soc. 127 (2005) 16090–16097.
[12]. H. She, Y. Chen, X. Chen, K. Zhang, Z. Wang and D.-L. Peng, J. Mater. Chem. 22 (2012) 2757–2765.
[13]. Z. Ban, Y. Barnakov, F. Li, V. Golub and C. O`Connor, J. Mater. Chem. 15 (2005) 4660–4662.
[14]. H.T. Zhang, J. Ding, G.M. Chow, M. Ran and J.B. Yu, Chem. Mater. 21 (2009) 5222–5228.
[15]. M. Tsuji, D. Yamaguchi, M. Matsunaga and K. Ikedo, Cryst. Growth Des. 11 (2011) 1995–2005.
[16]. Ju.A. Zakharov, N.K. Yeremenko, V.G. Dodonov, I.I. Obrazcova, A.N. Yeremenko. Chemistry for sustainable development 23 (2015) 177–182.
[17]. N.K. Yeremenko, V.G. Dodonov, I.I. Obraztsova, A.N. Yeremenko, Bulletin of Kemerovo State University, 2014, 59, 189 (in Russian).
[18]. V.G. Dodonov, Zeitschrift fur Kristallographie, New Crystal Structures, 1991, 4, 102.
[19]. J.F. Bondi, Rajiv Mistra, Xianglin Ke, Ian T. Sines and Raymond E. Schaak. Chem. Mater. 22 (2010) 3988–3994.